Materials & Design 217 (2022) 110634

Contents lists available at ScienceDirect

Materials & Design

journal homepage: www.elsevier.com/locate/matdes

New analytical model and 3D finite element simulation for improved pressure prediction of elastic compression stockings

Chongyang Ye [a], Rong Liu [a,b,*], Xinbo Wu [b], Fuyou Liang [c], Michael T.C. Ying [d], Jingyun Lv [e]

[a] Institute of Textiles and Clothing, The Hong Kong Polytechnic University, Hung Hom, Kowloon, Hong Kong Special Administrative Region
[b] Laboratory for Artificial Intelligence in Design, Hong Kong Science Park, New Territories, Hong Kong Special Administrative Region
[c] Department of Engineering Mechanics, Shanghai Jiao Tong University, Shanghai, China
[d] Department of Health Technology and Informatics, The Hong Kong Polytechnic University, Hung Hom, Hong Kong Special Administrative Region
[e] School of Fundamental Education, Beijing Polytechnic College, Beijing, China

HIGHLIGHTS

- A new analytic model and systematic experimental methods for determining three- dimensional mechanical properties of elastic compression materials are introduced.
- The experimentally validated finite element elastic-compression model can predict interface pressure between elastic compression stocking materials and contacted body.
- Application of three-dimensional material mechanical properties in knitted material simulation produced more agreement of pressure profiles to the measured results.
- The improved simulation precision of the finite element elastic-compression model contributes to pressure performance prediction and elastic material design.

GRAPHICAL ABSTRACT

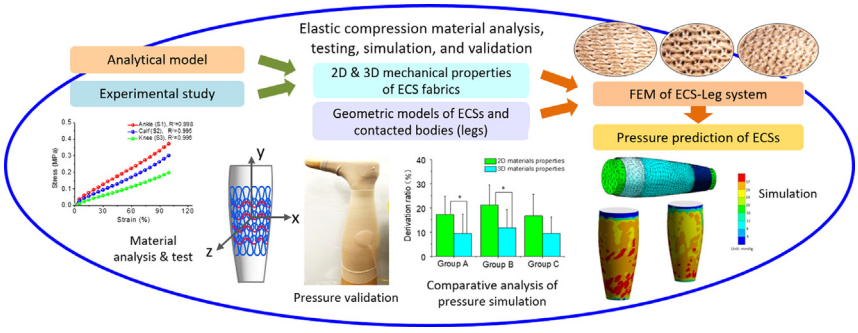

ARTICLE INFO

Article history:
Received 18 January 2022
Revised 21 March 2022
Accepted 5 April 2022
Available online 09 April 2022

Keywords:
Elastic compression materials
Mechanical properties
Pressure prediction
Finite element modeling
Compression stockings

ABSTRACT

Elastic compression stockings (ECSs) are essential for the prevention and treatment of venous disorders of the lower limbs. Finite element modeling (FEM) is an effective method for numerically analyzing ECS pressure performance for guiding ECS material design and pressure dose selection in treatment. However, existing FEM studies have primarily used the two-dimensional (2D) mechanical properties (i.e., properties along the wale and course directions) of ECS fabrics and ignored their three-dimensional (3D) mechanical properties (i.e., those along the thickness direction), causing deviations in pressure predictions. To address this limitation, the present study developed a new approach for determining the 3D mechanical properties of ECS fabrics through orthotropic theoretical analysis, analytical model development, FEM, and experimental testing and validation. The results revealed that the deviation ratios between the experimental and simulated pressure values of ECS fabrics was 19.3% obtained using the 2D material mechanical properties that was reduced to 10.3% obtained using the 3D material mechanical properties. Equivalently, the FEM simulation precision increased by 46.6%. These results indicate that the proposed approach can improve finite element analysis efficiency for ECS pressure

* Corresponding author at: Institute of Textiles and Clothing, The Hong Kong Polytechnic University, Hung Hom, Kowloon, Hong Kong Special Administrative Region.
E-mail address: rong.liu@polyu.edu.hk (R. Liu).

https://doi.org/10.1016/j.matdes.2022.110634

prediction, thus facilitating the functional design of elastic compression materials for improving compression therapeutic efficacy.

1. Introduction

Compression textiles have been commonly used to prevent and treat chronic venous insufficiency of the lower limbs through the delivery of controlled pressures and gradient distributions [1–3]. Elastic compression stockings (ECSs), as one type of commonly used compression textile, exert relatively high-pressure levels at the distal leg while gradually decreases toward the proximal leg. To date, ECSs have become an essential component of compression therapy for reducing venous hypertension [4], augmenting muscular pumping action, and promoting venous return [1,5]. However, high noncompliance rates [3] in ECS use have hindered their application in practice; such noncompliance is commonly due to complaints of pain, discomfort, or poor fit [6,7] and to side-effects such as ischemia or recurrence caused by excessive or insufficient pressures [8,9]. An effective assessment and prediction of material properties and pressure performance can facilitate ECS material design, pressure dose selection, and ECS applications in compression therapy.

Finite element modeling (FEM) has been used as a biomechanical approach [10,11] to analyze interactions between digitalized compression garments and the human body and visualize and predict garment pressure performance for facilitating pressure dose design and control [12,13]. Liu et al. constructed a finite element (FE) model to simulate ECS deformations and interface pressures at different heights and along with different directions of the lower limb [14]. Dai et al. applied FEM to analyze ECS-exerted skin pressure by assuming tubular compression materials to be orthotropic linear elasticity [15]. Ghorbani et al. used FEM to investigate knitted compression fabric structures and their effects on skin pressure and tissue stress [16] with a simulation error of approximately 19.64% compared with experimental results. Zhao et al. applied FEM to simulate upper limb skin pressure distributions and elastic fabric deformations caused by elastic sleeves [17]. Chassagne et al. applied FEM to analyze interface pressure and frictional properties between a viscoelastic medical compression bandage and the lower limbs [18]. Following it, investigation of mechanical relationships among fabric strain, Young's modulus, and pressure exerted on the FE bust by elastic sports vests was conducted [19]. Ye and Liu further analyzed and predicted mechanical transmission behaviors of compression garments within soft tissues and even vascular structures by using FEM [20]. In addition, FE modeling has been also applied in microscale material simulation. Dinh et al. applied FE model to predict mesostructured mechanical properties of knitted yarns and fabrics by utilizing hierarchical multiscale method [21]. Liu et al. applied parallelized explicit and implicit FE analysis to assess yarn scaled mechanical behavior of knitted textile [22] and adopted multiscale homogenization approach to predict macroscopic mechanical properties of the knitted textiles resulting from their underlying microstructures [23]. The findings of these studies enhance the understanding of the mechanical properties of knitted materials and pressure profiles of compression textiles. Nevertheless, the existing FE simulations on the microstructures of knitted yarns and fabrics have not revealed their effects on the corresponding pressure performance in a 3D-scale, and most of the existing FEM studies have assumed the compression textiles or garment layers to be orthotropic laminas and have considered only their mechanical properties along the fabric wale (warp or vertical) and course (weft or horizontal) directions [24,25] (Fig. 1) while ignoring their mechanical properties across the fabric thickness, which directly contribute to the normal pressure (dose) in practical applications.

ECSs are commonly fabricated by intermeshing ground and inlay yarns to form laid-in knitted loop structures [26]. Tubular ECS fabrics produce an orthotropic plane stress state along their wale and course directions when placed on a flat plane; when they are mounted onto the human body, their original plane stress state changes under stretching, bending, and shear forces, resulting in a complex three-dimensional (3D) stress plane. The contact condition varies with changes in the leg tissues and the pressure delivery status. Existing FEM studies on ECS–leg systems have primarily considered the two-dimensional (2D) mechanical properties of ECS fabrics (i.e., properties along the fabric wale and course directions only) in pressure simulations but ignored the mechanical properties and their variations along the fabric's thickness when worn. This simplification may affect the precision of simulated ECS pressure values. Accordingly, developing an effective approach for determining 3D mechanical properties in the thickness direction

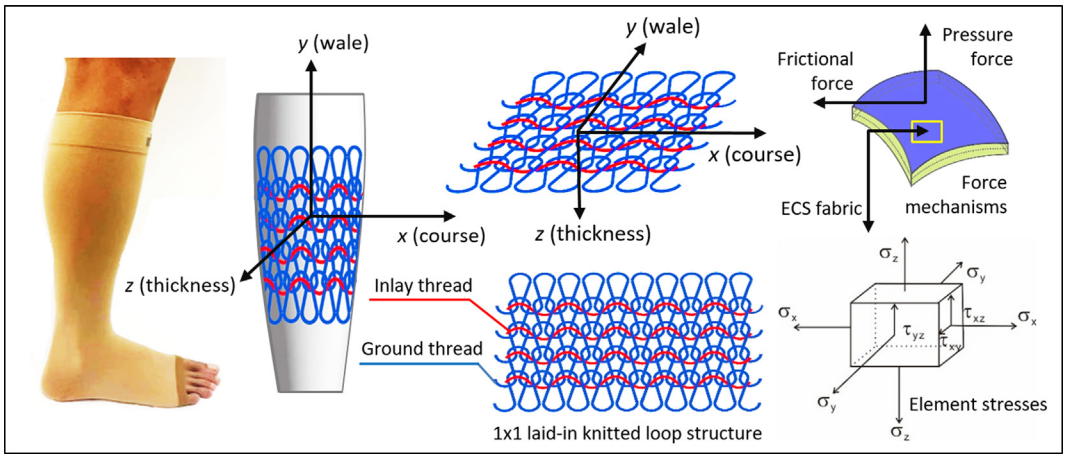

Fig. 1. The determined course, wale, and thickness directions of the ECS fabric with laid-in knitted loop structure in this study.

of ECS fabrics in addition to the wale and course directions is highly valuable for more realistically understanding the effects of ECS material properties on pressure performances; this can thus facilitate the functional design of ECSs to improve compression therapeutic efficacy.

FEM simulation of the mechanical properties of elastic fabrics under tension, shear, compression, and bending conditions commonly apply three essential elastic modulus parameters, namely E, v, G, which indicate tensile or compression stiffness, expansion or contraction deformation, and elastic shear stiffness, respectively [14,27]. To determine the elastic moduli of orthotropic compression fabrics, the Kawabata evaluation system (KES) [28] and the Instron testing system are usually applied to quantitatively identify the relationships between the loading forces and deformations of elastic fabrics. However, these existing instrumental tests are primarily performed along the wale and course directions in elastic fabrics. Few studies have investigated the elastic moduli of fabrics across their thickness, in part because determining G values along their thickness directions is challenging owing to their thin structures and few available testing instruments.

To address these limitations, the present study introduces a new approach for determining the elastic moduli of ECS fabrics on a 3D scale. This approach entails the integration of orthotropic theoretical analysis, model development, and experimental testing and validation. A new analytical model is derived to determine the elastic moduli of ECS fabrics along the thickness directions. By applying the 2D and 3D elastic moduli derived for ECS fabric samples through a developed FE model, we simulated the interface pressure values (doses and gradients) exerted by the ECS fabrics and verified the simulation results through comparisons with experimentally measured pressure values. The results indicate that the proposed approach can more realistically determine the 3D mechanical properties of ECS fabrics and improve the FEM simulation precision for ECS analysis, thus promoting pressure dose design, selection, and control in ECSs to improve compression therapy.

2. Materials and methods

2.1. Interaction between ECS fabrics and leg models

ECS fabrics are commonly assumed as orthotropic elastic materials because the mechanical properties along their course and wale directions are different [24]. During the dynamic interaction between ECSs and the lower limbs, ECS fabrics produce 3D deformations conforming to the surface curvature of the leg tissues (Fig. 1), resulting in the exertion of varying interface pressure and frictional force levels on the skin surface and deeper tissues to regulate venous hemodynamics. The essential elastic moduli of ECS fabrics (i.e., E, v, and G) predominantly govern the degree of fabric deformation and resultant biomechanical effects exerted on the lower limb. According to the RAL-GZ 387/1 standard (Medical Compression Hosiery Quality Assurance), the elongation of ECS fabrics along the circumference of the leg should range between 15% and 120%. It facilitates the maintenance of linear elasticity in stretching, the application of appropriate tension, recovery after repeated uses, and donning and doffing in practical use.

Hooke's law describes the linear relationship between the stress and strain of materials under a specific deformation condition (e.g., uniaxial tension, compression, shear, or bending; Figs. 1 and 2). It can be applied to analyze the mechanical parameters (E, v, G) of ECS fabrics and their variations under deformation when applied to the lower limbs. Eq. (1) presents the generalized Hooke's law [29],

$$\begin{bmatrix} \varepsilon_x \\ \varepsilon_y \\ \varepsilon_z \\ \gamma_{xy} \\ \gamma_{xz} \\ \gamma_{yz} \end{bmatrix} = \begin{bmatrix} S_{11} & S_{12} & S_{13} & S_{14} & S_{15} & S_{16} \\ S_{21} & S_{22} & S_{23} & S_{24} & S_{25} & S_{26} \\ S_{31} & S_{32} & S_{33} & S_{34} & S_{35} & S_{36} \\ S_{41} & S_{42} & S_{43} & S_{44} & S_{45} & S_{46} \\ S_{51} & S_{52} & S_{53} & S_{54} & S_{55} & S_{56} \\ S_{61} & S_{62} & S_{63} & S_{64} & S_{65} & S_{66} \end{bmatrix} \begin{bmatrix} \sigma_x \\ \sigma_y \\ \sigma_z \\ \tau_{xy} \\ \tau_{xz} \\ \tau_{yz} \end{bmatrix} \quad (1)$$

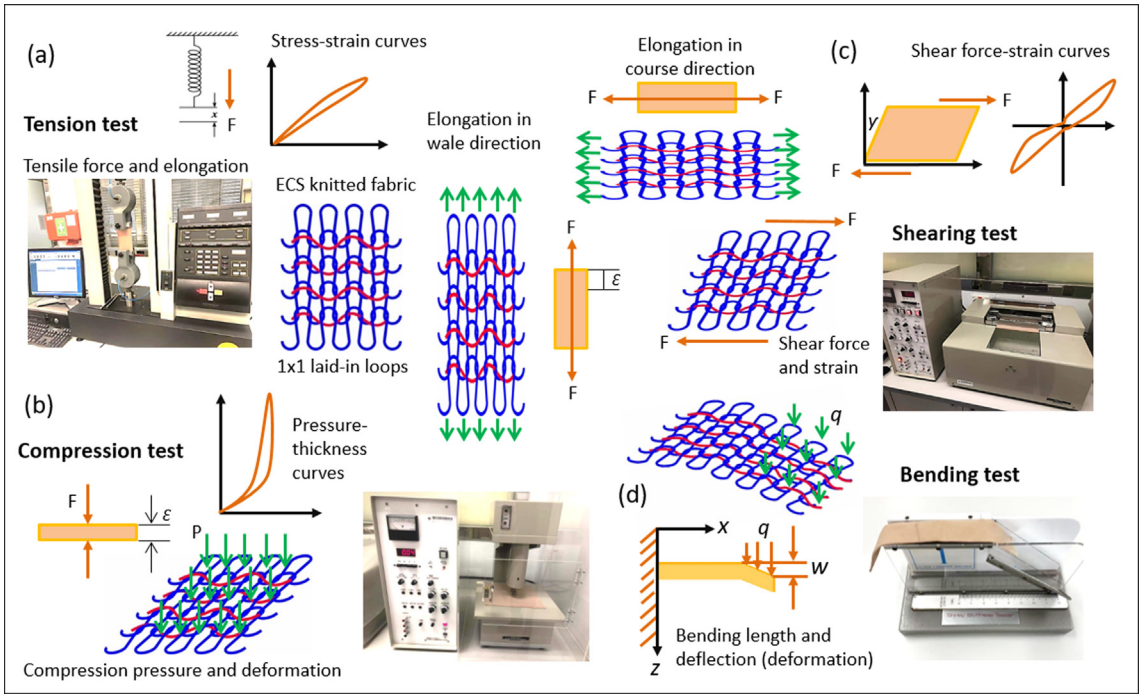

Fig. 2. Applied experimental testing system for determination of mechanical properties of ECS fabrics, including (a) uniaxial Instron 4411 tension testing for E_x, E_y, v_{xy}, v_{xz}, and v_{yz}; (b) compression testing (KES-FB3) for E_z, (c) shearing testing (KES-FB1) for G_{xy}; and (d) cantilever beam bending (shirley stiffness) testing for G_{xz} and G_{yz}.

where $[S_{ij}]$ is the orthotropic compliance matrix (OCM) of the ECS fabrics; ε_i and γ_{ij} are the normal strain and shear strain, respectively; and σ_i and τ_{ij} are the normal stress and shear stress, respectively. The OCM indicates the relationship between stress and strain [30], which can be determined by the orthogonal elastic moduli of ECS fabrics, as expressed in the following equation:

$$\begin{bmatrix} \varepsilon_x \\ \varepsilon_y \\ \varepsilon_z \\ \gamma_{xy} \\ \gamma_{xz} \\ \gamma_{yz} \end{bmatrix} = \begin{bmatrix} \frac{1}{E_x} & -\frac{v_{yx}}{E_y} & -\frac{v_{zx}}{E_z} & 0 & 0 & 0 \\ -\frac{v_{xy}}{E_x} & \frac{1}{E_y} & -\frac{v_{zy}}{E_z} & 0 & 0 & 0 \\ -\frac{v_{xz}}{E_x} & -\frac{v_{yz}}{E_y} & \frac{1}{E_z} & 0 & 0 & 0 \\ 0 & 0 & 0 & \frac{1}{G_{xy}} & 0 & 0 \\ 0 & 0 & 0 & 0 & \frac{1}{G_{xz}} & 0 \\ 0 & 0 & 0 & 0 & 0 & \frac{1}{G_{yz}} \end{bmatrix} \begin{bmatrix} \sigma_x \\ \sigma_y \\ \sigma_z \\ \tau_{xy} \\ \tau_{xz} \\ \tau_{yz} \end{bmatrix} \quad (2)$$

Here, x, y, and z are the three principal stress directions (Fig. 1) that indicate the corresponding course, wale, and thickness directions of the knitted ECS fabric under examination, respectively. The orthogonal relationship between E and v along the three coordinate directions can be expressed as follows:

$$-\frac{v_{xy}}{E_y} = -\frac{v_{yx}}{E_x}; -\frac{v_{xz}}{E_z} = -\frac{v_{zx}}{E_x}; -\frac{v_{yz}}{E_z} = -\frac{v_{zy}}{E_y} \quad (3)$$

Thus, the 3D E (E_x, E_y, and E_z), v (v_{xz}, v_{yz}, and v_{xy}), and G (G_{xy}, G_{xz}, and G_{yz}) values of ECS fabrics can be determined.

2.2. Analytical model for determining 3D mechanical properties of ECS fabrics

E_x, E_y, and E_z indicate the 3D tensile stiffnesses of an ECS fabric, which can be determined using stress–strain curves along the course, wale, and thickness directions of the fabric [27] through uniaxial tensile testing and compression tests (Fig. 2a and b). In a uniaxial tensile test, the tensile stress along the wale direction σ_y is equal to zero, and the compressive stress along the thickness direction σ_z is equal to zero when the ECS fabric is stretched along the course direction x. Thus, the OCM of the ECS fabric can be presented as follows:

$$E_x = \frac{\sigma_x}{\varepsilon_x} \quad (4)$$

where σ_x and ε_x denote the tensile stress and tensile strain, respectively, of the ECS fabric along the course direction. When the ECS fabric is stretched along the wale direction y or compressed along the thickness direction z, the OCMs of ECS fabric can be written as follows,

$$E_y = \frac{\sigma_y}{\varepsilon_y}; E_z = \frac{\sigma_z}{\varepsilon_z} \quad (5)$$

where ε_y and ε_z are the tensile strain along the wale direction and compressive strain along the thickness direction, respectively. In addition, v is a crucial mechanical parameter that describes the ECS fabric expansion or contraction deformation along the direction perpendicular to the loading (compression or stretching) direction [27,31]. v_{xy}, v_{xz}, and v_{yz} along the wale, course, and thickness directions can be determined by using uniaxial tensile tests. The OCMs for v_{xy}, v_{xz}, and v_{yz} are presented as follows:

$$v_{xy} = -\frac{\varepsilon_y E_x}{\sigma_x}; v_{xz} = -\frac{\varepsilon_z E_x}{\sigma_x}; v_{yz} = -\frac{\varepsilon_z E_y}{\sigma_y} \quad (6)$$

G indicates the elastic shear stiffness, which can be defined as the ratio of shear stress to shear strain [27,32]. A shear test can be used to measure the shear stress and shear strain within a plane (Fig. 2c). The OCM for G in a 3D plane can be expressed as follows:

$$G_{xy} = \frac{\tau_{xy}}{\gamma_{xy}}; G_{xz} = \frac{\tau_{xz}}{\gamma_{xz}}; G_{yz} = \frac{\tau_{yz}}{\gamma_{yz}} \quad (7)$$

where τ_{xy}, τ_{xz}, and τ_{yz} represent the shear stress along the course–wale (x–y), course–thickness (x–z), and wale–thickness (y–z) planes, respectively, γ_{xy}, γ_{xz}, and γ_{yz} represent the shear strains in these planes, respectively. In practical tests, directly measuring τ_{xz}, τ_{yz}, γ_{xz}, and γ_{yz} in the x–z and y–z planes are difficult because ECS fabrics are usually thin (<1.2 mm) and few instruments are available for direct testing. Therefore, an analytical model based on bending measurements was developed in the present study to facilitate the derivation of G_{xz} and G_{yz} in the x–z and y–z planes, respectively.

In the bending test of the proposed model, an ECS fabric is regarded as a cantilever beam structure in which one end is supported but the other end extends horizontally [33]. The bending load is caused by the fabric's own weights, and its deflection (i.e., the bending deformation along the loading direction) can be measured as illustrated in Fig. 2d, where h and b_x denote the original thickness and edge width, respectively, of the ECS fabric, and l denotes the edge length of the deformed ECS fabric during bending. The relationship among G_{yz} and G_{xz}, bending loading, and bending deformation along the z direction can be derived using the Airy stress function [34]. The Airy stress function is a semi-inverse method for determining the loading conditions for plane stress or plane strain problems based on the mechanical equilibrium equation [29]. It can be expressed for isotropic elastic materials as follows:

$$\frac{\partial^4 U}{\partial y^4} + \frac{\partial^4 U}{\partial z^2 \partial y^2} + \frac{\partial^4 U}{\partial z^4} = 0 \quad (8)$$

The orthotropic Airy stress function can be derived on the basis of the isotropic Airy stress function as follows:

$$S_{33}\frac{\partial^4 U}{\partial y^4} + (2S_{23} + S_{66})\frac{\partial^4 U}{\partial z^2 \partial y^2} + S_{22}\frac{\partial^4 U}{\partial z^4} = 0 \quad (9)$$

where S_{33}, S_{23}, S_{22}, and S_{66} are the coefficients corresponding to the compliance matrix (Eq. (2)); U is the orthotropic Airy stress function.

In this cantilever beam bending test in the proposed model, the bending stress σ_z of the ECS fabric is generated by its bending loading q (self-weight), which is a constant. σ_z is a function of z. U can be further determined by applying Eq. (10) through the use of Eq. (9):

$$U = \frac{y^2}{2}f(z) + yf_1(z) + f_2(z) \quad (10)$$

Eq. (10) can be substituted into Eq. (9) as follows:

$$\frac{1}{2E_y}\frac{d^4 f(z)}{dz^4}y^2 + \frac{1}{E_y}\frac{d^4 f_1(z)}{dz^4}y + \frac{1}{E_y}\frac{d^4 f_2(z)}{dz^4} + \left(\frac{1}{G_{yz}} - \frac{2v_{yz}}{E_y}\right)\frac{d^2 f(z)}{dz^2} = 0 \quad (11)$$

According to Eq. (11), all items must be zero to satisfy the Airy stress function, which is expressed as follows,

$$\frac{d^4 f(z)}{dz^4} = 0; \frac{d^4 f_1(z)}{dz^4} = 0; \left(\frac{1}{G_{yz}} - \frac{2v_{yz}}{E_y}\right)\frac{d^2 f(z)}{dz^2} = 0 \quad (12)$$

Consequently, Eq. (12) can be derived as follows:

$$\begin{aligned} f(z) &= Ay^3 + By^2 + Cy + D; \\ f_1(z) &= Ey^3 + Fy^2 + Gy; \\ f_2(z) &= Hy^5 + Iy^4 + Jy^3 + Ky^2 \end{aligned} \quad (13)$$

where A to K are the undetermined coefficients. Thus, the determined U can be derived as follows:

$$U = \frac{y^2}{2}(Az^3 + Bz^2 + Cz + D) + y(Ez^2 + Fz^2 + Gz) + Hz^5 + Iz^4 + Jz^3 + Kz^2 \quad (14)$$

On the basis of the Airy stress function, the relationship between the normal stress, shear stress, and stress function of the ECS fabric during bending can be derived as follows:

$$\begin{aligned}&\sigma_y = \tfrac{\partial^2 U}{\partial z^2} = \tfrac{y^2}{2}(6Az + 2B) + y(6Ez + 2F) + 20Hz^3 + 12Iz^2 + 6Jz + 2K;\\ &\sigma_z = \tfrac{\partial^2 U}{\partial y^2} = 2(z^3 + Bz^2 + Cz + D);\\ &\tau_{yz} = -\tfrac{\partial^2 U}{\partial z \partial y} = -y(6Az^2 + 4Bx + 2C) - (3Ez + 2Fz + G)\end{aligned} \quad (15)$$

The boundary conditions of the ECS fabric under bending deformation can be expressed as follows:

$$\begin{aligned}&(\sigma_z)_{z=-\frac{h}{2}} = -\tfrac{q}{b_y};\ (\tau_{yz})_{z=-\frac{h}{2}} = 0;\ (\sigma_z)_{z=\frac{h}{2}} = 0;\ (\tau_{yz})_{z=\frac{h}{2}} = 0;\\ &(\tau_{yz})_{y=0} = 0;\ \int_{-\frac{h}{2}}^{\frac{h}{2}} (\sigma_y)_{y=0} dz = 0;\ \int_{-\frac{h}{2}}^{\frac{h}{2}} z(\sigma_y)_{y=0} dz = 0\end{aligned} \quad (16)$$

Furthermore, the stress components of the ECS fabric can be derived using Eq. (16):

$$\begin{aligned}&\sigma_y = -\tfrac{qy^2 z}{2I} - \tfrac{q(2\upsilon_{yz} - \frac{E_y}{G_{yz}})}{2I}(\tfrac{1}{3}z^3 - \tfrac{h^2}{20}z);\\ &\sigma_z = -\tfrac{q}{b_y 2}(1 - \tfrac{3z}{h} + \tfrac{4z^3}{h^3});\\ &\tau_{yz} = \tfrac{q}{2I}(z^2 - \tfrac{h^2}{4})y\end{aligned} \quad (17)$$

where σ_y and σ_z represents the normal stresses along the wale and thickness directions of the ECS fabric, respectively. τ_{yz} represents the shear stress in the y–z plane; and I represents the inertia moment. On the basis of Eq. (2), the normal strain and shear strain can be derived as follows:

$$\begin{aligned}&\varepsilon_y = -\tfrac{qy^2 z}{2E_y I} - \tfrac{q(2\upsilon_{yz} - \frac{E_y}{G_{yz}})}{2E_y I}(\tfrac{1}{3}z^3 - \tfrac{h^2}{20}z) + \tfrac{q\upsilon_{zy}}{2b_y E_z}(1 - \tfrac{3z}{h} + \tfrac{4z^3}{h^3});\\ &\varepsilon_z = -\tfrac{q}{2b_y E_z}(1 - \tfrac{3z}{h} + \tfrac{4z^3}{h^3}) + \tfrac{q\upsilon_{yz} y^2 z}{2E_y I} - \tfrac{\upsilon_{yz} q(2\upsilon_{yz} - \frac{E_y}{G_{yz}})}{2E_y I}(\tfrac{1}{3}z^3 - \tfrac{h^2}{20}z);\\ &\gamma_{yz} = \tfrac{q}{2G_{yz} I}(z^2 - \tfrac{h^2}{4})y\end{aligned} \quad (18)$$

where ε_y and ε_z are normal strains along the wale and thickness directions, respectively, and γ_{yz} is the shear strain in the y–z plane. Consequently, the bending deformation of the ECS fabric along the y and z directions can be expressed as follows:

$$\begin{aligned}&\upsilon = -\tfrac{qy^3 z}{6E_y I} - \tfrac{qP}{2E_y I}(\tfrac{1}{3}z^3 - \tfrac{h^2 z}{20})y + \tfrac{q\upsilon_{zy}}{2b_y E_z}(1 - \tfrac{3z}{h} + \tfrac{4z^3}{h^3})y + ff(z);\\ &w = -\tfrac{q}{2b_y E_z}(z - \tfrac{3z^2}{2h} + \tfrac{z^4}{h^3}) + \tfrac{q\upsilon_{yz} y^2 z^2}{4E_y I} - \tfrac{\upsilon_{yz} q(2\upsilon_{yz} - \frac{E_y}{G_{yz}})}{2E_y I}(\tfrac{1}{12}z^4 - \tfrac{h^2 z^2}{40}) + \varphi(y)\end{aligned} \quad (19)$$

where υ and w denote the bending deformation (displacement) along the y and z directions, respectively; correspondingly, $ff(z)$ and $\varphi(y)$ denote the undetermined function to satisfy the relationship between the strain and deformation.

According to Eqs. (18) and (19), the following relationship can bederived:

$$\frac{d\varphi(y)}{dy} + \frac{q\upsilon_{yz} yz^2}{2E_y I} - \frac{qy^3}{6E_y I} - \frac{q(2\upsilon_{yz} - \frac{E_y}{G_{yz}})}{2E_y I}(z^2 - \frac{h^2}{20})y + \frac{q\upsilon_{zy}}{2E_z}(\frac{3}{b_y h} + \frac{z^2}{I})y + \frac{dff(z)}{dz} = \frac{q}{2G_{yz} I}(z^2 - \frac{h^2}{4})y \quad (20)$$

The boundary condition of the bending deformation of the ECS fabric can be expressed as follows:

$$(\upsilon)_{y=l,z=0} = 0;\ (w)_{y=l,z=0} = 0;\ (\frac{\partial w}{\partial y})_{y=l,z=0} = 0 \quad (21)$$

On the basis of Eq. (21), the separation-of-variables method [35] can be applied to determine the relationship between the fabric bending deformation along the z direction w_y, q, and G_{yz}, as indicated in the following expression:

$$w_y = \frac{qL^4}{8E_y I_y} - \frac{q(2\upsilon_{yz} - \frac{E_y}{G_{yz}})L^2 h^2}{80E_y I_y} - \frac{3q\upsilon_{yz} L^2}{4b_y E_y h} - \frac{qh^2 L^2}{16G_{yz} I_y} \quad (22)$$

Similarly, the relationship between w_x, q, and G_{xz} can be expressed as follows:

$$w_x = \frac{qL^4}{8E_x I_x} - \frac{q(2\upsilon_{xz} - \frac{E_x}{G_{xz}})L^2 h^2}{80E_x I_x} - \frac{3q\upsilon_{xz} L^2}{4b_x E_x h} - \frac{qh^2 L^2}{16G_{xz} I_x} \quad (23)$$

On the basis of Eqs. (22) and (23), G in x–z and y–z planes of the ECS fabric can be determined as follows:

$$\begin{aligned}&G_{xz} = -\frac{qh^2 L^2}{20I_x\left(w_x - \frac{qL^4}{8E_x I_x} + \frac{3q\upsilon_{xz} L^2}{4E_x b_x h} + \frac{q\upsilon_{xz} L^2 h^2}{40E_x I_x}\right)}\\ &G_{yz} = -\frac{qh^2 L^2}{20I_y\left(w_y - \frac{qL^4}{8E_y I_y} + \frac{3q\upsilon_{xz} L^2}{4E_x b_y h} + \frac{q\upsilon_{yz} L^2 h^2}{40E_y I_y}\right)}\end{aligned} \quad (24)$$

Based on the developed analytical model, the relationships among the mechanical properties (E, υ, and G), stress, strain, and deformation of the ECS fabrics have been determined. Based on the determined relationships, the values of E, υ, and G can be further obtained with the aid of experimental testing (Fig. 2) as shown in Section 2.3, in detail.

2.3. Preparation of ECS fabric samples and testing of their physical and mechanical properties

Nine samples of tailor-made knitted tubular ECS fabrics that were footless and composed of interlooped ground and inlay yarns were prepared and equipped with 1 × 1 laid-in loop structures (Fig. 1) [26] to provide pressure gradients at the ankle, calf, and knee portions. Polyamide double-covered Lycra yarns with a linear density of 40D were used as the ground threads that were knitted into loops to provide substrate fabric thickness, and polyamide-double covered Lycra yarns with a linear density of 240D were used as the inlay threads that were laid into the substrate structure without knitting into loops during the same knitting cycle to regulate the fabric tension and pressure doses. The geometric structures of laid-in knitted loops were stretched, compressed, and bended under the action of mechanical forces (Fig. 2). Table 1 presents the physical characteristics of the prepared ECS fabric samples. Sample codes S1/S2/S3, S4/S5/S6, and S7/S8/S9 indicate the knee, calf, and ankle segments of the corresponding A, B, and C groups of the studied ECS fabrics. Prior to testing, all samples were placed in an environmentally controlled laboratory (relative humidity: 65% ± 2%, temperature 21 ± 1 °C) for 48 h to reach equilibrium.

The microstructural and tensile and shearing deformation of the ECS fabrics are illustrated in Fig. 3. ECS fabric samples measuring 100 mm (length) × 75 mm (width) per piece were prepared for tensile tests using an Instron 4411 system (Norwood, MA, USA; Fig. 2a). The tensile tests were performed to produce stress–strain curves along the course (x) and wale (y) directions of the prepared ECS fabrics at a standard tensile rate of 10 mm/s; these tests were conducted in accordance with the ASTM D4964-96 standard. On the basis of the derived stress–strain curves, E_x and E_y were calculated using Eqs.4 and 5. To determine E_z along the thickness direction, a Vernier caliper was used for thickness measurement. Stress–strain curves reflecting the relationship between compressive pressure and compressive

Table 1
Physical characteristics of the prepared knitted tubular ECS fabric samples.

Group	Section	Sample code	Courses/inch	Wale/inch	Thickness (mm)	Mass density (g/m^2)
A	Knee	S1	44	37	0.75	319
	Calf	S2	48	40	0.76	365
	Ankle	S3	55	46	0.72	413
B	Knee	S4	43	36	0.70	286
	Calf	S5	46	38	0.74	308
	Ankle	S6	50	39	0.77	370
C	Knee	S7	54	42	0.77	330
	Calf	S8	59	45	0.75	372
	Ankle	S9	72	58	0.76	436

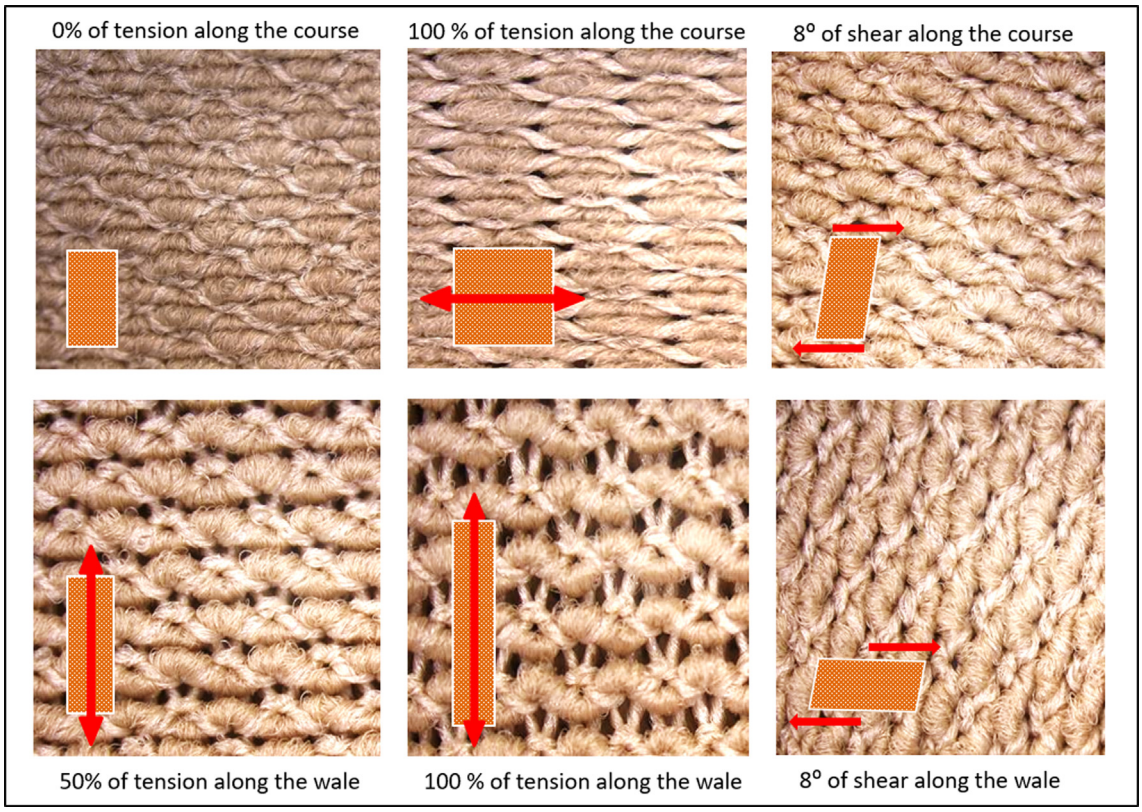

Fig. 3. Microstructures of laid-in knitted ECS fabrics under different mechanical deformation in testing.

thickness were obtained using the KES-FB3 testing system (Kawabata evaluation system, Kyoto, Japan); thus, E_z could be determined using Eq. (5) (Fig. 2b).

To determine v for the tested ECS fabric samples on a 3D scale, the contraction of the fabrics during transverse deformation under uniaxial tension was measured using the Vernier caliper. On the basis of the measured contraction and stretching, v_{xy}, v_{xz}, and v_{yz} were calculated using Eq.6. Shear stress–strain curves were obtained for the ECS fabrics by testing the fabric samples with a size of 200 mm × 200 mm per piece on a pure shear test (KES-FB1) at an 8° shear angle (Fig. 2c). Subsequently, G_{xy} was calculated using Eq.7. To determine G_{xz} and G_{yz}, the weights (kg) of ECS fabric samples measuring 200 mm × 25 mm were measured using a BP211D electronic balance (Sartorius, Germany), and their w values (mm) were determined using a Shirley Stiffness tester (Testex, China) in accordance with the ASTM-D 1388-2014 standard (Fig. 2d). Thus, G_{xz} and G_{yz} of the studied ECS fabrics were obtained by applying Eq. (24).

2.4. Construction of FE models to analyze interface pressure exerted by ECS fabric samples

To numerically analyze the interface pressure exerted by the ECS fabrics on the basis of their 2D and 3D mechanical properties, this study developed new FE models. The geometric FE leg models were constructed based on our three previously fabricated wooden leg models (WL-I, WL-II, WL-III) for Asian bodies. The shaped wooden leg models have rigid surface, round cross-sections, and three different sizes as shown in Table 2 and Fig. 4. The geometric FE ECS models were constructed based on the actual dimensions of the ECS fabric samples (Fig. 4a) by using ANSYS Workbench Design Modeler software (v19.2, ANSYS, Pennsylvania, Pittsburgh, USA). The 2D (E_x, E_y, v_{xy}, and G_{xy}) and 3D (E_x, E_y, E_z, v_{xy}, v_{xz}, v_{yz}, G_{xy}, G_{xz}, and G_{yz}) material mechanical properties were used as inputs in the developed FE ECS models. The LS-Dyna explicit dynamic solver was used in Ansys for FE model through applying central difference method to discrete dynamic equation. The FE leg models were con-

Table 2
Geometric characteristics of the developed FE leg and ECS models in the FEM.

	Circumference (C, cm)				Height (H, cm)		
ECS samples	C1	C2	C3	C4	H1	H2	H3
Group A	17.6	18.9	16.2	14.8	5.0	14.0	5.0
Group B	21.7	23.7	19.7	16.7	6.0	12.0	6.0
Group C	23.9	26.4	19.6	16.3	5.0	13.0	6.0
Leg models	C1	C2	C3	C4	H1	H2	H3
WL-I	29.6	31.9	26.0	18.0	9.0	9.0	9.0
WL-II	34.0	35.9	29.4	20.3	9.0	9.0	9.0
WL-III	37.8	39.3	32.8	22.5	9.0	9.0	9.0

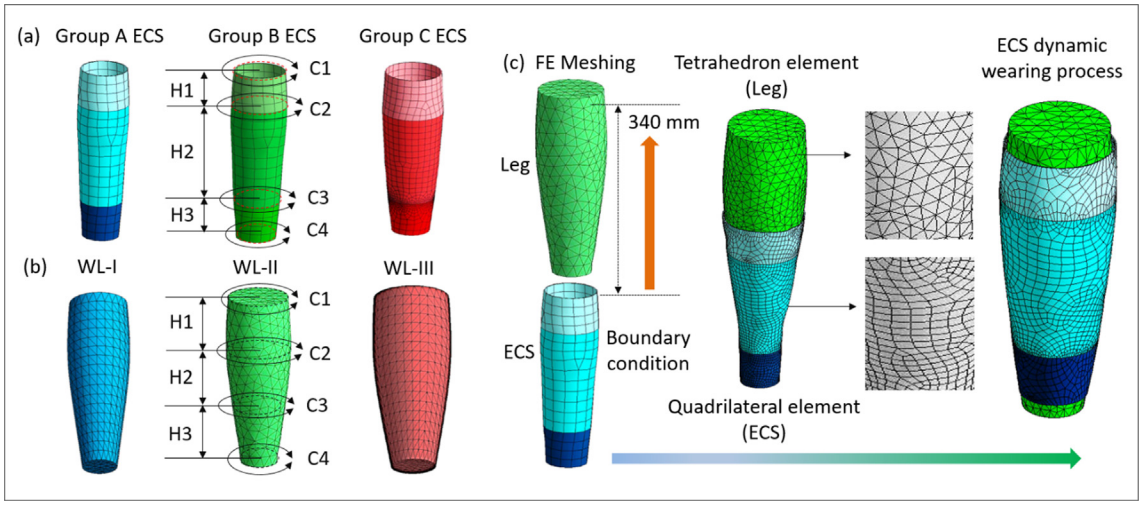

Fig. 4. The developed geometric models of (a) FE ECSs and (b) FE legs, and (c) the meshing and boundary conditions applied in the FEM.

structed under the assumption that the wooden leg was isotropic elastic materials with E and v values of 500 MPa and 0.4, respectively [36]. The FE ECS and FE leg models were meshed using linear quadrilateral elements and tetrahedrons elements with approximately 30,000 and 50,000 nodes, respectively (Fig. 3c). To examine the meshing independence of the developed FE model, different meshing sizes (4, 6, and 8 mm per element) were applied to the FE leg model (WL-II) using the FE ECS of Group C. The results indicated that the meshing size of 6 mm per element produced the best meshing quality with a value of 0.842, thus this meshing size was adopted to simulate interface pressure induced by ECSs. The constructed FE ECS and leg models were imported into ANSYS workbench LS-Dyna for FE analysis under a 4-core, 16 GB RAM, 512 GB SSD hardware computing system. The frictional nonlinear contact has been applied in the developed FE model based on the Augmented Lagrange equation, where the sliding resistance is proportional to the coefficient of the friction, and the free separation between the ECS and the wooden leg models is unimpeded. The boundary conditions of ECS deformation were determined based on an approximately 340-mm longitudinal displacement of the ECS fabric samples, in accordance with practical usage conditions (Fig. 4c). The upper and bottom surfaces of the wooden leg model was fixed with the zero displacements of all nodes at x, y, and z directions in the boundary. The top edge of ECS can dynamically slide freely from the distal to the proximal leg model longitudinally. The center of the cross-sectional leg and ECS models were coincident to ensure ECS to slide exactly along the leg for achieving an alignment. The circumference of the ECS can deform freely with tubular fabric stretching with variation of leg volume. The total degree of freedoms (DOFs) of the built FE ECS-leg model was approximately 275000, where the DOFs of every node were six. The boundary conditions restricted the six DOFs of the upper and bottom surfaces of the FE leg model and the one DOF along the longitudinal direction of the FE ECS model for every node. Both 2D and 3D material mechanical parameters were applied to simulate the interface pressures by ECS fabrics.

2.5. Validation of the effectiveness of the 3D ECS mechanical properties in pressure prediction

To verify the simulated pressure values, an air-filled pneumatic pressure-sensing system was applied to directly detect the interface pressure between the wooden leg models and the ECS fabrics by placing the flexible pressure sensor probe with a diameter of 5 cm and a thickness of 0.2 mm (PicoPress, Microlab Elettronica Sas, Italy; pressure range: 0–189 mmHg; deviation within ± 1 mmHg) [37] at 36 typical sites around the 4 directions (anterior, media, lateral, and posterior) and 3 height levels (ankle, calf, and knee) of the three tested wooden leg models (WL-I, WL-II, WL-III), sequentially. The average pressure value detected by the pressure sensor probe over the circular area on the wooden leg model was recorded. Similarly, in the Ansys numerical simulation, the interface pressure was also defined as the average pressure value obtained over the same circular area with a diameter of 5 cm on the FE leg model surface. The testing positions at the FE leg model and the corresponding wooden leg model were identical to ensure a consistent study condition between the simulated and the measured interface pressure. The deviations between the simulated and the measured pressure values were compared to verify the effectiveness of the 3D material mechanical properties in ECS pressure prediction (Fig. 5).

Fig. 6 presents the study flowchart, including orthotropic theoretical analysis, analytic model development, FEM, and experimental testing and validation. The constructed analytical models integrated with the experimental tests were used to establish the relationships between material elastic moduli, strain, and force

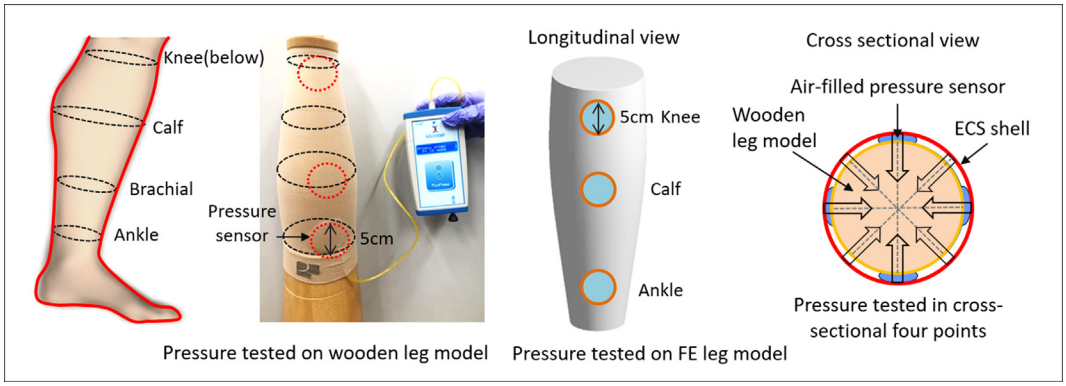

Fig. 5. Experimental setting of pressure validation testing.

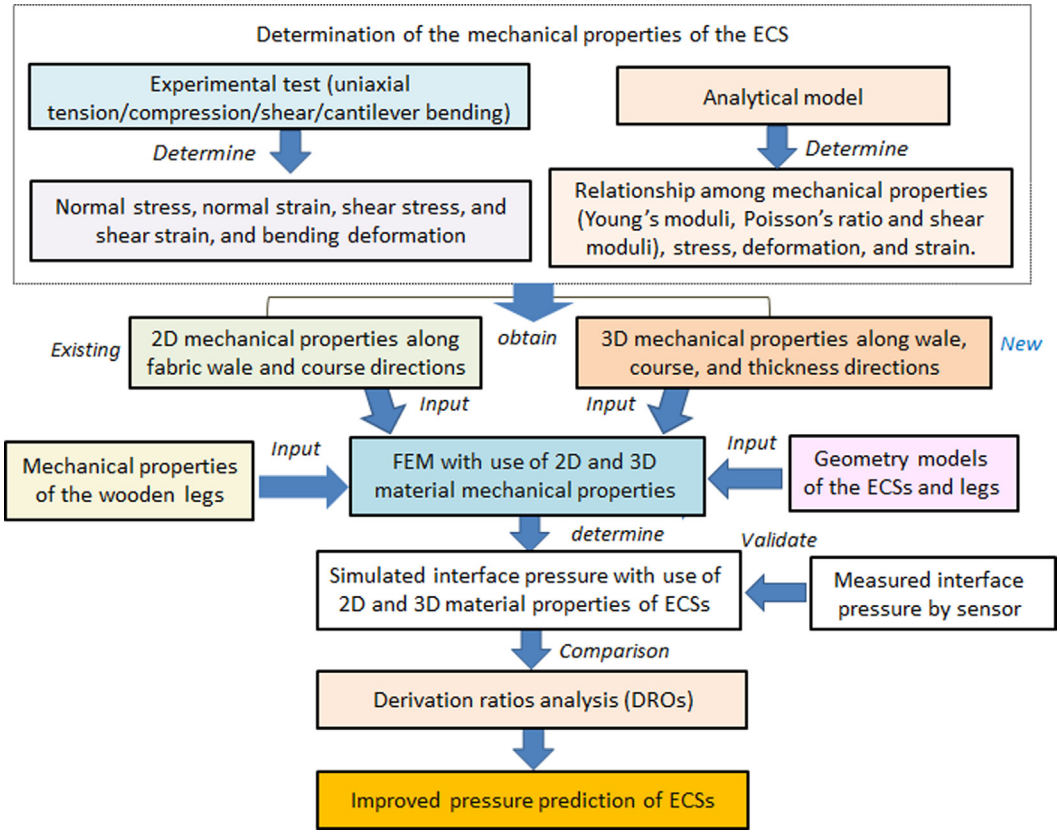

Fig. 6. Workflow of this proposed study.

loading behaviors of ECS fabrics. Mechanical properties of ECS fabrics and contacted bodies and geometric models of the contacted bodies are the input parameters for FEM. Interface pressure effects caused by using 2D and 3D mechanical properties of ECS fabrics were comparatively studied in the deviation ratios (DROs) analysis.

3. Results and discussion

3.1. Mechanical properties of ECS fabrics

Table 3 presents the 2D and 3D mechanical properties of the ECS fabric samples. Fig. 7 illustrates the corresponding stress–strain curves along with linear regression coefficients. The goodness-of-fit values obtained for the tested ECS fabric samples were >0.95 (R^2 > 0.95) at stretching ratios of 0%–100%. Overall, the derived E_x values were greater than the E_y and E_z values, implying that the ECS fabrics produced shorter stretches along the course direction to exert greater squeezing forces in order to deliver higher interface pressure levels to the leg models. The derived υ_{xy}, υ_{xz}, and υ_{yz} values for the studied ECS fabrics were approximately 0.25. Overall, the derived G_{xy} values were greater than the derived G_{yz} and G_{xz} values, indicating that the ECS fabrics could produce larger shear deformation levels under the same shear stress in the x–y plane than in x–z and y–z planes.

3.2. Simulated interface pressure values between ECS fabrics and wooden leg models

Fig. 8 displays the simulated (using 2D and 3D material mechanical properties) interface pressure values between the ECS fabrics and wooden leg models for all three studied groups of ECS fabrics. In general, the gradient profiles of the simulated

Table 3
The determined mechanical properties of the studied ECS fabrics in 2D and 3D scales.

Group	Sections	Sample code	E_x (MPa)	E_y (MPa)	E_z (MPa)	v_{xy}	v_{xz}	v_{yz}	G_{xy} (MPa)	G_{xz} (MPa)	G_{yz} (MPa)
A	Knee	S1	*0.24*	*0.20*	0.08	*0.26*	0.24	0.26	*0.11*	0.05	0.04
	Calf	S2	*0.35*	*0.30*	0.09	*0.25*	0.24	0.25	*0.14*	0.06	0.04
	Ankle	S3	*0.45*	*0.35*	0.10	*0.23*	0.23	0.22	*0.17*	0.08	0.05
B	Knee	S4	*0.40*	*0.14*	0.05	*0.25*	0.27	0.27	*0.12*	0.02	0.01
	Calf	S5	*0.43*	*0.18*	0.06	*0.25*	0.29	0.24	*0.12*	0.03	0.01
	Ankle	S6	*0.48*	*0.27*	0.05	*0.26*	0.26	0.26	*0.15*	0.05	0.02
C	Knee	S7	*0.35*	*0.14*	0.03	*0.24*	0.29	0.30	*0.11*	0.03	0.01
	Calf	S8	*0.49*	*0.22*	0.04	*0.25*	0.24	0.25	*0.13*	0.03	0.02
	Ankle	S9	*0.60*	*0.22*	0.04	*0.25*	0.25	0.27	*0.21*	0.05	0.02

* All above listed columns are the determined 3D mechanical properties those were applied to the FEM of ECS fabrics.
The columns with Italic date are the determined 2D mechanical properties those were applied to the FEM of ECS fabrics.

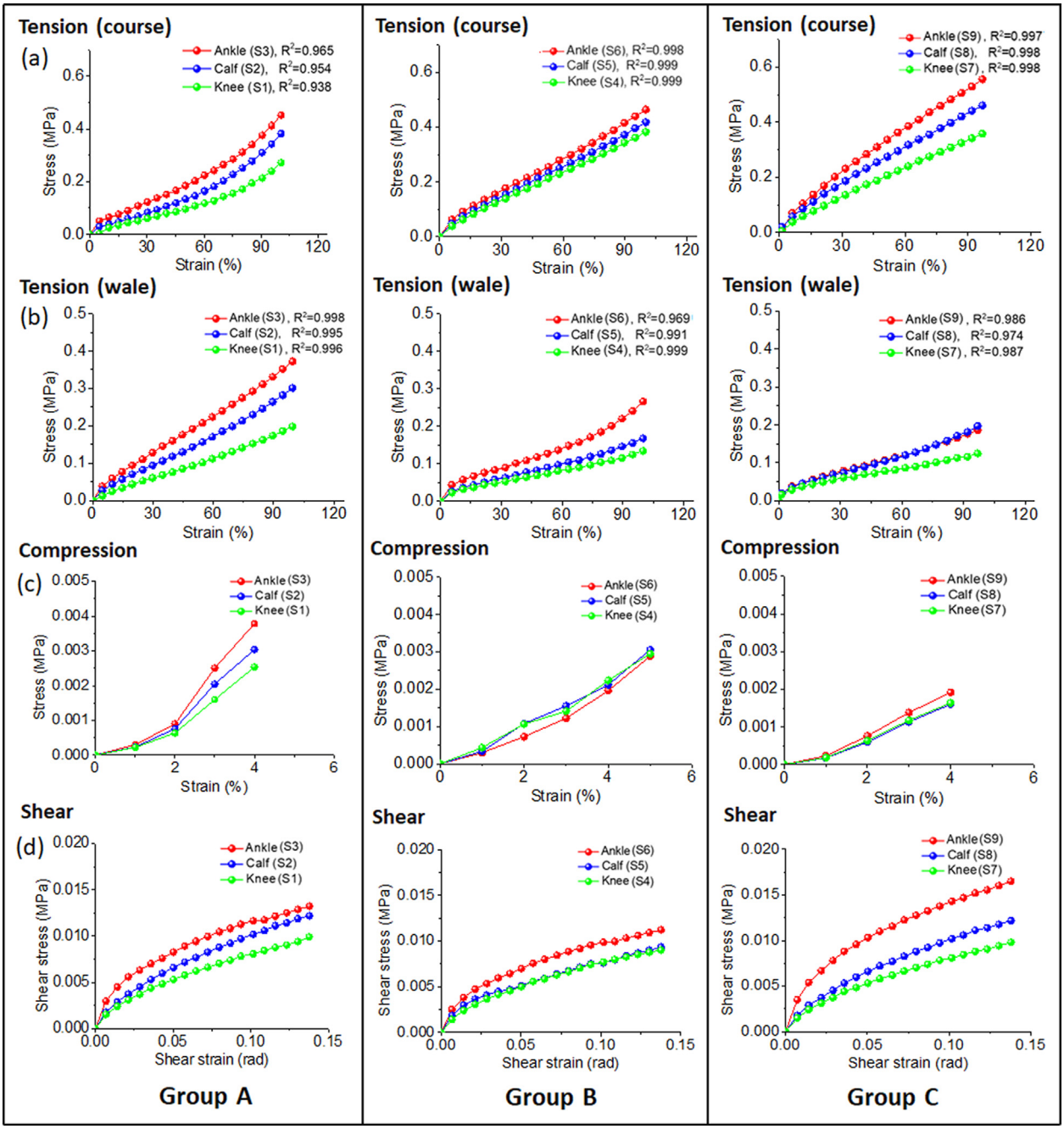

Fig. 7. The determined stress–strain curves of the studied ECS fabrics by experimental tests in terms of (a) tension in course direction, (b) tension in wale direction, (c) compression at thickness direction, and (d) shearing at course-wale plane.

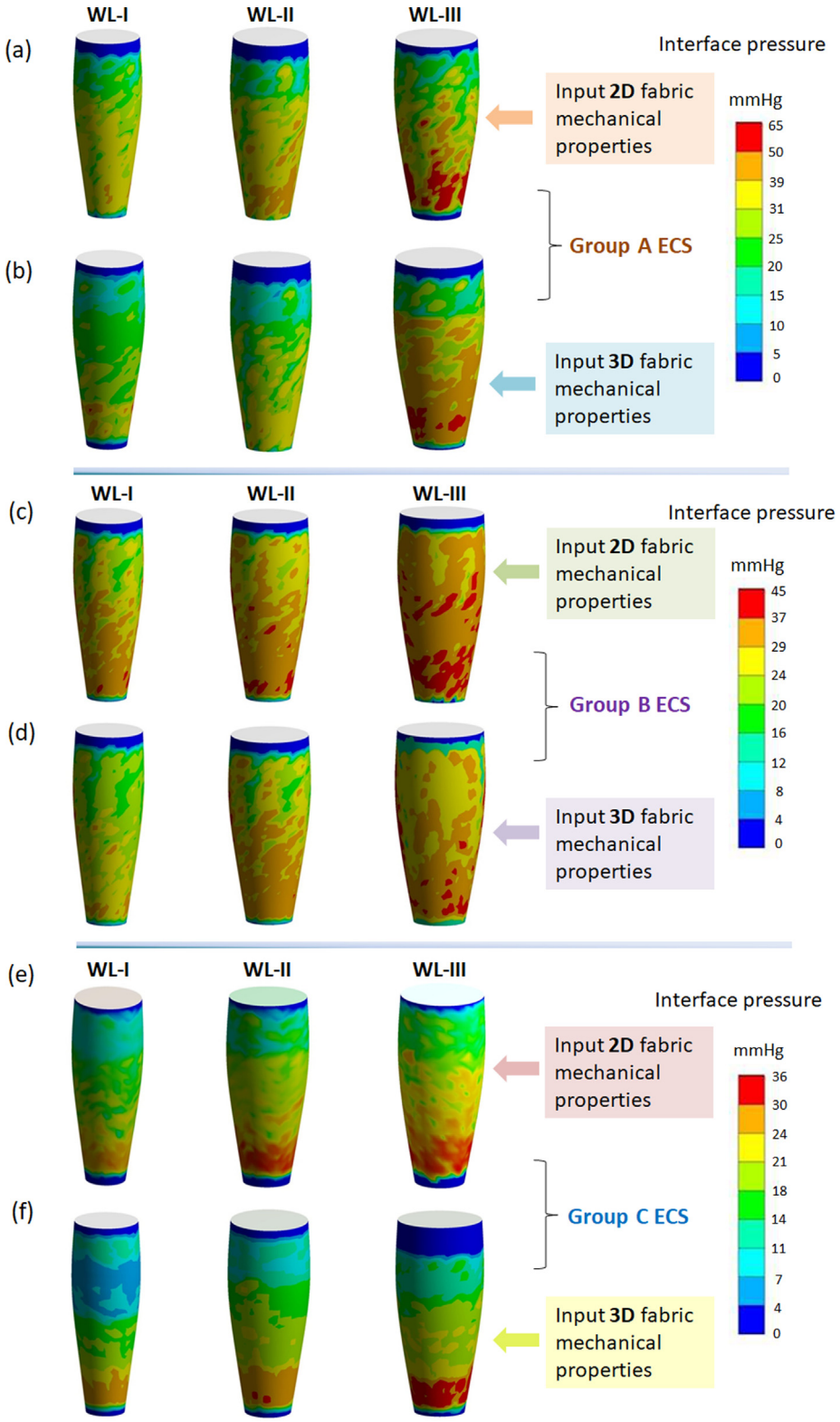

Fig. 8. The simulated interface pressure profiles applied by the different groups of the studied ECSs when their 2D and 3D material mechanical properties were applied, respectively.

pressure values along the leg models decrease gradually. Specifically, the highest pressure was exerted at the ankle, decreasing gradually toward the knee; this profile is consistent with the basic design principle for ECSs in medical treatment. Both 2D and 3D material properties could be used to reveal the pressure gradient profiles of the studied ECS fabrics. Overall, the pressure values simulated for the ECS fabrics with the 2D material mechanical properties were greater than those simulated for the ECS fabrics with the 3D material mechanical properties by approximately 9.2%. For example, the simulated interface pressure between the WL-I leg

Table 4
Results of meshing independence examination.

Meshing size (mm)	Element number	Meshing quality	Interface pressure (mmHg)		
			Ankle	Calf	Knee
8	18,207	0.836	28.4 ± 4.0	20.9 ± 1.6	12.0 ± 4.2
6	46,507	0.842	27.0 ± 2.8	20.0 ± 1.3	11.1 ± 3.4
4	95,150	0.836	27.2 ± 2.6	19.9 ± 1.5	11.0 ± 3.5

model and the Group C ECS fabrics with the 2D material mechanical properties was 25.6 mmHg at the ankle, 20.2 mmHg at the calf, and 14.7 mmHg at the knee, and that obtained for the ECS fabrics with the 3D material mechanical properties were 22.3 mmHg at the ankle, 16.0 mmHg at the calf, and 9.3 mmHg at the knee. These ECS fabrics could thus be assigned to the Class-II pressure category (medium) for treatment of moderate venous disorders such as varicose veins and leg swelling in application [38,39]. To further verify the effectiveness of the use of 2D and 3D material mechanical properties in pressure performance prediction, a series of experiments were conducted to compare the simulated and the experimental data as described in Section 3.3.

Table 4 shows the comparison results of meshing independence examination among different meshing sizes (4, 6, and 8 mm per element) tested in the developed FEM. All three mesh densities of the FE models produced the similar levels of the simulated interface pressure, indicating that these meshing densities are high enough to enable meshing-numerical solutions. Relatively, our applied meshing size of 6 mm per element presented the highest meshing quality value of 0.842, that is, the developed FEM can effectively reflect pressure profiles exerted by the studied ECSs.

3.3. Validation of the simulated interface pressure values against experimental data

Fig. 9 illustrates the comparison between the pressure values simulated using the 2D or 3D material mechanical properties with the experimental pressure values. The results indicated that the pressure values simulated for the ECS fabrics with the 3D material mechanical properties were in closer agreements with the experimental pressure values in general, especially for the Group C of ECS samples applied to the WL-I, WL-II, and WL-III leg models.

Table 5 presents the differences between the simulated and measured interface pressure values. When the ECS fabrics with 2D material mechanical properties were applied to the WL-I, WL-II, and WL-III models, the DROs between the simulated and measured pressure values were approximately 26.7%, 14.0%, and 17.2%, respectively, while the corresponding DROs were reduced to 13.7%, 10.4%, and 6.7% when ECSs fabrics with 3D mechanical properties were applied to the same groups of leg models. That is, the average DROs between the simulated and measured pressure values decreased from approximately 19.3% for the ECS fabrics with the 2D material mechanical properties to 10.3% for the ECS

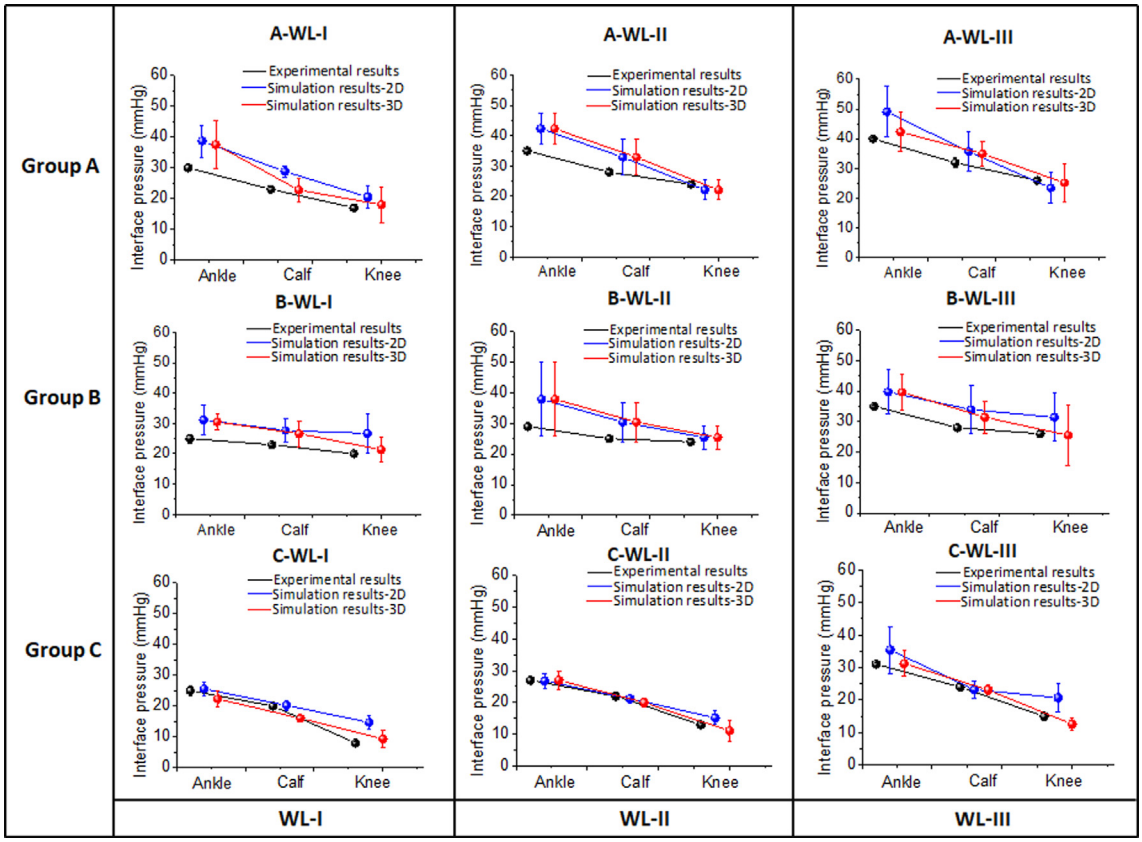

Fig. 9. Comparison between the simulated and measured interface pressures when ECSs materials (groups A, B, and C) were applied with 2D and 3D mechanical properties to the different sized wooden leg models.

Table 5
Details on DROs of the simulated and the measured pressure values by using 2D and 3D material mechanical properties of ECS fabrics, respectively.

ECS samples	Simulated pressure by ECSs with 2D or 3D material mechanical properties					Measured pressure Experimented test
	2D			3D		
		Simulated pressure (mmHg) (pressure gradient %)	DRO (%)	Simulated pressure (mmHg) (pressure gradient %)	DRO (%)	Measured pressure (mmHg) (pressure gradient %)
Group A-WL-I	Ankle	38.7 ± 5.2 (100%)	29.0	37.5 ± 7.7 (100%)	25.0	30 ± 0.7 (100%)
	Calf	28.8 ± 1.8 (75%)	25.2	22.8 ± 3.8 (61%)	0.9	23 ± 0.5 (77%)
	Knee	20.5 ± 3.6 (53%)	20.6	18.0 ± 5.9 (48%)	5.9	17 ± 0.7 (57%)
Group A-WL-II	Ankle	42.3 ± 5.2 (100%)	20.9	42.3 ± 5.0 (100%)	20.9	35 ± 0.5 (100%)
	Calf	32.9 ± 5.9 (78%)	17.5	30.2 ± 4.2 (71%)	7.9	28 ± 0.7 (80%)
	Knee	22.1 ± 3.3 (52%)	7.9	25.2 ± 4.2 (60%)	5.0	24 ± 0.5 (69%)
Group A-WL-III	Ankle	49.1 ± 8.5 (100%)	22.8	42.8 ± 6.6 (100%)	7.0	40 ± 0.4 (100%)
	Calf	35.7 ± 6.6 (73%)	11.6	35.0 ± 4.1 (82%)	9.4	32 ± 1.6 (80%)
	Knee	23.5 ± 5.1 (48%)	9.6	25.2 ± 6.4 (59%)	3.1	26 ± 0.6 (65%)
Group B-WL-I	Ankle	31.1 ± 4.8 (100%)	24.4	30.5 ± 2.6 (100%)	22.0	25 ± 1.4 (100%)
	Calf	27.7 ± 3.9 (89%)	20.4	26.6 ± 4.2 (87%)	15.7	23 ± 0.4 (92%)
	Knee	26.7 ± 6.4 (86%)	33.5	21.4 ± 4.2 (70%)	7.0	20 ± 0.8 (80%)
Group B-WL-II	Ankle	37.9 ± 12.1 (100%)	30.7	33.9 ± 4.6 (100%)	16.9	29 ± 0.9 (100%)
	Calf	30.4 ± 6.4 (80%)	21.6	29.6 ± 4.7 (87%)	18.4	25 ± 0.7 (86%)
	Knee	25.4 ± 3.9 (67%)	5.8	24.1 ± 5.6 (71%)	0.4	24 ± 0.5 (83%)
Group B-WL-III	Ankle	39.7 ± 7.2 (100%)	13.4	39.6 ± 5.7 (100%)	13.1	35 ± 0.5 (100%)
	Calf	33.9 ± 7.9 (85%)	21.1	31.4 ± 5.2 (79%)	12.1	28 ± 0.8 (80%)
	Knee	31.4 ± 7.9 (79%)	20.8	25.5 ± 9.9 (64%)	1.9	26 ± 0.7 (74%)
Group C-WL-I	Ankle	25.6 ± 2.2 (100%)	2.4	22.3 ± 2.4 (100%)	10.8	25 ± 1.6 (100%)
	Calf	20.2 ± 1.6 (79%)	1.0	16.0 ± 1.0 (72%)	20.0	20 ± 1.0 (80%)
	Knee	14.7 ± 2.1 (57%)	83.8	9.3 ± 2.9 (42%)	16.3	8 ± 0.5 (32%)
Group C-WL-II	Ankle	26.8 ± 2.2 (100%)	0.7	27.0 ± 2.8 (100%)	0	27 ± 1.0 (100%)
	Calf	21.2 ± 0.9 (81%)	3.6	20.0 ± 1.3 (74%)	9.1	22 ± 0.9 (82%)
	Knee	15.2 ± 2.1 (57%)	16.9	11.1 ± 3.4 (41%)	14.6	13 ± 0.4 (48%)
Group C-WL-III	Ankle	35.4 ± 7.2 (100%)	14.2	31.2 ± 3.9 (100%)	0.6	31 ± 0.5 (100%)
	Calf	23.2 ± 3.6 (66%)	3.3	23.1 ± 1.5 (74%)	3.8	24 ± 1.0 (77%)
	Knee	20.7 ± 4.3 (59%)	38.0	13.6 ± 2.0 (44%)	9.3	15 ± 0.8 (48%)

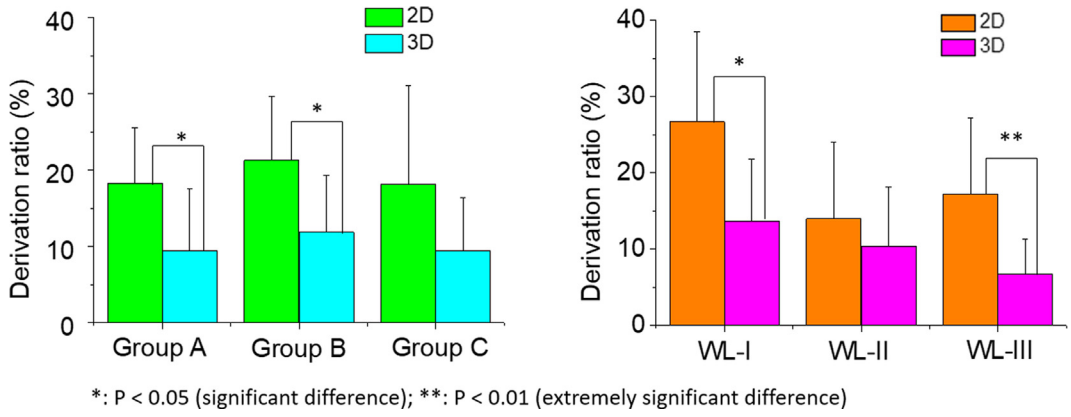

Fig. 10. Comparison on the DROs (%) between the use of 2D and 3D material mechanical properties when being applied with three different groups of ECS samples on three different sizes of leg models.

fabrics with the 3D material mechanical properties (Fig. 10). Equivalently, the simulation precision increased by approximately 46.6%.

The ECS–leg interaction system is in a 3D stress state if the fabric stresses along the wale, course, and thickness directions are all nonzero. Previous research assumed that ECS fabric are orthotropic laminas in a plane stress state [40], without considering material mechanical properties along the thickness directions, which could lead to overestimations or underestimations in the predicted pressure values. The results of the present study reveal that the use of ECS fabrics with 3D material mechanical properties could more realistically predict actual conditions, thus leading to FEM-based pressure simulation results to be more consistent with actual pressure values. To further analyse the effects of changing the material mechanical properties on pressure prediction performance, we used wooden leg models with a round cross section and a rigid surface; this enabled us to focus on the material properties and their variations in the simulations while ignoring other factors influencing pressure values, such as irregular leg surface curvatures and heterogeneous tissue stiffness. In a future study, we will include more complex contact conditions such as biologic leg models with uneven surfaces and varying tissue properties to further estimate

the effects of modelled ECS material properties on the corresponding pressure prediction performance.

E, *v*, and *G* are elastic moduli that are commonly used to indicate the mechanical properties of compression fabrics in FEM through integrating 2D orthotropic analysis theories and Instron or Kawabata biaxial tensile and shearing testing. In one of our previous studies [14], the measured *E* values of 1 × 1 laid-in knitted ECS fabrics along the wale direction were 0.278, 0.214, and 0.150 MPa at the ankle, calf, and knee, respectively, and along the course direction, the values were 0.197, 0.150, and 0.103 MPa at the ankle, calf, and knee, respectively. Its results indicated that with use of these 2D material properties of ECS fabric in the FEM, the DROs between the simulated and measured interface pressure values at the ankle, calf, and knee presented approximately 44.0%, 16.5%, and 20.4%, respectively. Through optimization, our recent FE study [20] using the similar structured knitted ECS fabrics with 2D mechanical properties reduced these DROs to approximately 15.5%, 15.2%, and 18.1% at the ankle, calf, and knee, respectively. However, these error ranges remain above 15%. In contrast to methods as aforementioned, this new approach proposed herein applies mechanical properties derived along the thickness direction (E_z, v_{xz}, v_{yz}, G_{xz}, and G_{yz}) in addition to those derived along the wale and course directions (E_x, E_y, v_{xy}, and G_{xy}) for pressure simulation through FEM, which reduced the DROs to be 10.3% generally, implying that the use of material thickness properties can affect the simulated normal pressure magnitudes exerted by ECS fabrics on the applied contacted body (leg models).

Overall, our analytical approach for determining shear moduli along the thickness direction (G_{xz}, G_{yz}) by using the Airy stress function and experimental tests provides a new solution for obtaining essential material properties of thin, soft, and elastic compression fabrics. The Airy stress function is commonly used to solve 2D linear elastic problems to characterize material stress, strain, and deformation [29,41]. For example, Rastgoo et al. applied an isotropic Airy stress function to construct mathematical models for estimating the 2D stress distribution of a cantilever beam under parabolic loading [42]. In contrast to previous studies, this proposed analytical approach applies the orthotropic Airy stress function and cantilever testing [43] to determine the cantilever bending stress, strain, and deformation of ECS fabrics, thus enabling the quantification of the relationship between bending deformation *w*, bending loading *q*, and shear modulus *G*. This approach provides an effective way for obtaining the 3D tensile, shear, and bending properties of ECSs, enabling mechanical simulations to more closely reflect the actual status of deformed fabrics in an ECS–leg interaction system. In future studies, we will further apply this approach to investigate compression fabrics composed of different elastic materials and simulate their corresponding pressure performance for individual treatments by using more complex FE models with irregular body geometries and elastic heterogeneous tissue structures.

Numerical modeling has become a highly important approach to provide solutions to investigate complex working mechanisms of functional textiles and apparel as well as their interactions with the human body, especially for those studies requiring repeated trials and material preparations or lacking effective experimental methods to test or verify. Interface pressure applied by the compression textiles (e.g., ECSs) on the human body (e.g., leg) forms a mechanical continuum with a larger area, which is hard to be tested by using the current pressure sensing system with single or several sensors or probes; moreover, human body is irregular in geometry and heterogeneous in tissue properties, using pressure contact sensors cannot directly detect pressure values at each anatomic site and their resultant stress and deformation within soft tissues. The application of FE modeling contributes to holistically investigating pressure contact condition and more complex interactions between garment system and the contacted body those experimental measurements cannot address. The findings of the numerical modeling in this study can facilitate material and product designers, engineers, and researchers to effectively analyze and evaluate design ergonomics and applicability for improved functional performance of compression materials and textiles.

4. Conclusions

This study developed a new approach for determining the mechanical properties of ECS fabrics in 3D stress planes based on the developed analytical model. Through the integrated Airy stress function and cantilever beam bending testing, the shear properties of ECS fabrics in the course–thickness and wale–thickness planes were determined. On the basis of orthotropic theory, FEM, and experimental testing, nine critical mechanical properties were obtained, including three-dimensional Young's moduli, Poisson's ratios, and shear moduli along the wale, course, and thickness directions of ECS fabrics, and their effects on pressure magnitudes (doses) and distributions (gradients) were simulated. The simulated pressure values were validated against experimental data obtained using a pressure-sensing system. The results indicate the applicability of the proposed approach for ECS pressure prediction. The approach improves the FEM-based simulation precision for ECS fabrics and affords substantially reduced DROs. The contribution of this study is the provision of an operable and reliable pressure prediction method, which can guide the design of ECSs with favorable mechanical properties and the determination of the elastic moduli of compression materials; this can thus enhance the understanding of the mechanisms underlying the interactions between elastic compression textiles and the human body, thereby facilitating compression material optimization and pressure dose control to achieve improved compression therapeutic efficacy.

Declaration of Competing Interest

The authors declare that they have no known competing financial interests or personal relationships that could have appeared to influence the work reported in this paper.

Acknowledgement

This work was supported by the General Research Fund (GRF) of University Grants Committee (UGC) through project PolyU252153/18E, the Laboratory for Artificial Intelligence in Design through project RP1-5 Innovation and Technology Fund (Hong Kong Special Administrative Region) through project RP1-5, Departmental General Research Fund of the Hong Kong Polytechnic University through project G-UAHB, and Youth Foundation of Beijing Polytechnic College through project BGY2021KY-05QT.

Data Availability Statement

The raw/processed data required to reproduce these findings cannot be shared at this time as the data also forms part of an ongoing study.

References

[1] R. Liu, X. Guo, T.T. Lao, T.J. Little, A critical review on compression textiles for compression therapy: textile-based compression interventions for chronic venous insufficiency, Text. Res. J. 87 (9) (2017) 1121–1141, https://doi.org/10.1177/0040517516646041.

[2] C.R. Lattimer, E. Kalodiki, M. Azzam, G. Geroulakos, Haemodynamic performance of low strength below knee graduated elastic compression

stockings in health, venous disease, and lymphedema, Eur. J. Vasc. Endovasc. 52 (1) (2016) 105–112, https://doi.org/10.1016/j.ejvs.2016.04.001.
[3] R. Liu, T.T. Lao, T.J. Little, X.B. Wu, X. Ke, Can heterogeneous compression textile design reshape skin pressures? A fundamental study, Text. Res. J. 88 (17) (2018) 1915–1930, https://doi.org/10.1177/0040517518779254.
[4] H. Partsch, Compression therapy: clinical and experimental evidence, Ann. Vasc. Dis. 5 (4) (2012) 416–422, https://doi.org/10.3400/avd.ra.12.00068.
[5] G. Mosti, H. Partsch, Duplex scanning to evaluate the effect of compression on venous reflux, Int. Angiol. 29 (5) (2010) 416–420. https://europepmc.org/article/med/20924344.
[6] S. Raju, K. Hollis, P. Neglen, Use of compression stockings in chronic venous disease: patient compliance and efficacy, Ann. Vasc. Surg. 21 (6) (2007) 790–795, https://doi.org/10.1016/j.avsg.2007.07.014.
[7] S.F. Tandler, Challenges faced by healthcare professionals in the provision of compression hosiery to enhance compliance in the prevention of venous leg ulceration, EWMA J. 16 (1) (2016) 29–33.
[8] B. Chemani, R. Halfaoui, Influence of pressure from compression textile bands: their uses in the treatment of venous human leg ulcers, Int. J. Phys. Sci. 9 (2014) 146–153, https://doi.org/10.5897/IJPS2014.4117.
[9] M. Perrin, Skin necrosis as a complication of compression in the treatment of venous disease and in prevention of venous thromboembolism, Phlebolymphology. 15 (2008) 27–30.
[10] C. Simoneau, P. Terriault, B.Jetté, M. Dumas, V. Brailovski, Development of a porous metallic femoral stem: design, manufacturing, simulation and mechanical testing, Mater. Des. 114 (2017), 546–556. doi.org/10.1016/j.matdes.2016.10.064.
[11] X. Ding, S.H. Liao, X.H. Zhu, H.M. Wang, B.J. Zou, Effect of orthotropic material on finite element modeling of completely dentate mandible, Mater. Des. 84 (2015) 144–153, https://doi.org/10.1016/j.matdes.2015.06.091.
[12] R. Dan, Z. Shi, Dynamic simulation of the relationship between pressure and displacement for the waist of elastic pantyhose in the walking process using the finite element method, Text. Res. J 91 (13–14) (2021) 1497–1508, https://doi.org/10.1177/0040517520981741.
[13] R. Liang, J. Yip, W. Yu, L. Chen, N.M. Lau, Numerical simulation of nonlinear material behaviour: application to sports bra design, Mater. Des. 183 (2019) 108177, https://doi.org/10.1016/j.matdes.2019.108177.
[14] R. Liu, Y.L. Kwok, Y. Li, T.T. Lao, X. Zhang, X.Q. Dai, A three-dimensional biomechanical model for numerical simulation of dynamic pressure functional performances of graduated compression stocking (GCS), Fiber. Polym. 7 (4) (2006) 389–397, https://doi.org/10.1007/BF02875771.
[15] X.Q. Dai, R. Liu, Y. Li, M. Zhang, Y.L. Kwok, Numerical simulation of skin pressure distribution applied by graduated compression stockings, in: Computational Textile, Springer, Berlin, Heidelberg, 2007, pp. 301–309.
[16] E. Ghorbani, H. Hasani, R.J. Nedoushan, N. Jamshidi, Finite element modeling of the compression garments structural effect on the pressure applied to leg, Fiber. Polym. 21 (3) (2020) 636–645, https://doi.org/10.1007/s12221-020-9542-3.
[17] L.H. Zhao, J. Yu, S. Zhang, C.Y. Li, A three-dimensional biomechanical model for prediction of garment pressure in pressure therapy for burn patients, Therm. Sci. 24 (4) (2020) 2357–2365, https://doi.org/10.2298/TSCI2004357Z.
[18] F. Chassagne, J. Molimard, R. Convert, P. Giraux, P. Badel, Numerical model reduction for the prediction of interface pressure applied by compression bandages on the lower leg, IEEE. T. Bio-Med. Eng. 65 (2) (2017) 449–457, https://doi.org/10.1109/TBME.2017.2774598.
[19] H. Liu, D.S. Chen, Q.F. Wei, P. Ruru, A study of the relationship between clothing pressure and garment bust strain, and Young's modulus of fabric, based on a finite element model, Text. Res. J. 81 (13) (2011) 1307–1319, https://doi.org/10.1177/0040517510399961.
[20] C.Y. Ye, R. Liu, Biomechanical prediction of veins and soft tissues beneath compression stockings using fluid-solid interaction model, Int. J. Biol. Biomed. 14 (10) (2020) 285–290.
[21] T.D. Dinh, O. Weeger, S. Kaijima, S.K. Yeung, Prediction of mechanical properties of knitted fabrics under tensile and shear loading: mesoscale analysis using representative unit cells and its validation, Compos. Part B-Eng. 148 (2018) 81–92, https://doi.org/10.1016/j.compositesb.2018.04.052.
[22] D. Liu, S. Koric, A. Kontsos, Parallelized finite element analysis of knitted textile mechanical behavior, J. Eng. Mater. Technol. 141(2) (2019) 021008, doi.org/10.1115/1.4041869.
[23] D. Liu, S. Koric, A. Kontsos, A multiscale homogenization approach for architectured knitted textiles, J. Appl. Mech. 86 (11) (2019) 1–27, https://doi.org/10.1115/1.4044014.
[24] J.Y. Zhou, Y. Li, J. Lam, X.Y. Cao, The poisson ratio and modulus of elastic knitted fabrics, Text. Res. J. 80 (18) (2010) 1965–1969, https://doi.org/10.1177/0040517510371864.
[25] K.W. Fong, S.Q. Li, R. Liu, A new geometric model of laid-in weft-knitted fabrics, Text.Res.J 91 (17–18) (2021) 2087–2105, https://doi.org/10.1177/0040517521992765.
[26] R. Liu, T.T. Lao, S.X. Wang, Impact of weft laid-in structural knitting design on fabric tension behavior and interfacial pressure performance of circular knits, J. Eng. Fibers Fabr. 88 (17) (2013) 96–107, https://doi.org/10.1177/155892501300800404.
[27] A. Bedford, K.M. Liechti, Mechanics of Materials, second ed., Cham, Springer Switzerland, 2020.
[28] C.M. Carr, Investigation of the effect of water repellent finishes on the mechanical properties of textiles using the kawabata evaluation system for fabrics, J. Coat. Fabr. 18 (2) (1988) 106–113, https://doi.org/10.1177/152808378801800205.
[29] T.G. Sitharam, L. Govindaraju, Theory of Elasticity, first ed., Springer Singapore, 2021.
[30] J.P. Yang, W.Z. Chen, Y.H. Dai, H.D. Yu, Numerical determination of elastic compliance tensor of fractured rock masses by finite element modeling, Int. J. Rock. Mech. Min. 70 (2014) 474–482, https://doi.org/10.1016/j.ijrmms.2014.06.007.
[31] H. Gercek, Poisson's ratio values for rocks, Int. J. Rock. Mech. Min. 44 (1) (2007) 1–13, https://doi.org/10.1016/j.ijrmms.2006.04.011.
[32] H. Wang, X. Liu, H. Zhang, P. Apostolidis, S. Erkens, A. Skarpas, Micromechanical modelling of complex shear modulus of crumb rubber modified bitumen, Mater. Des. 188 (2020) 108467, https://doi.org/10.1016/j.matdes.2019.108467.
[33] F.P. Beer, Mechanics of Materials, eighth ed., McGraw-Hill Education, New York, 2020.
[34] T. Van, A new fracture mechanics theory for orthotropic materials like wood, Eng. Fract. Mech. 74 (5) (2007) 771–781, https://doi.org/10.1016/j.engfracmech.2006.06.015.
[35] K. Schöbel (Ed.), An Algebraic Geometric Approach to Separation of Variables, Springer Fachmedien Wiesbaden, Wiesbaden, 2015.
[36] R.J. Alves, M.D. Magalhaes, E.V. Carrasco, Determination of the transverse Young's modulus (TYM) of wood by means of an input power technique, Constr. Build. Mater. 42 (2013) 11–21, https://doi.org/10.1016/j.conbuildmat.2012.12.061.
[37] R. Liu, J.D. Liu, T.T. Lao, M. Ying, X.B. Wu, Determination of leg cross-sectional curvatures and application in pressure prediction for lower body compression garments, Text. Res. J. 89 (10) (2019) 1835–1852, https://doi.org/10.1177/0040517518779246.
[38] C. Jungbeck, I. Thulin, C. Darenheim, L. Norgren, Graduated compression treatment in patients with chronic venous insufficiency: a study comparing low and medium grade compression stockings, Phlebology 12 (4) (1997) 142–145, https://doi.org/10.1177/026835559701200405.
[39] R. Liu, X. Guo, Q.J. Peng, L. Zhang, T.T. Lao, T. Little, J.D. Liu, E. Chan, Stratified body shape-driven sizing system via three-dimensional digital anthropometry for compression textiles of lower extremities, Text. Res. J. 88 (18) (2018) 2055–2075, https://doi.org/10.1177/0040517517715094.
[40] M. Gotoh, A theory of plastic anisotropy based on a yield function of fourth order (plane stress state)—I, Int. J. Mech. Sci. 19 (9) (1977) 505–512, https://doi.org/10.1016/0020-7403(77)90043-1.
[41] Q. Jiang, Z.D. Zhou, J.B. Chen, F.P. Yang, The method of fundamental solutions for two-dimensional elasticity problems based on the Airy stress function, Eng. Anal. Bound. Elem. 130 (2021) 220–237, https://doi.org/10.1016/j.enganabound.2021.05.021.
[42] A. Rastgoo, A. Amirian, Estimating the stresses in cantilever beam loaded by a parabolically distributed load with Airy stress functions, Int. J. Mech. Mater. Des. 3 (3) (2006) 253–264, https://doi.org/10.1007/s10999-007-9028-0.
[43] N.J. Abbott, The measurement of stiffness in textile fabrics, Text. Res. J. 21 (6) (1951) 435–441.